Flattening of asperities during biaxial in-plane deformation – Full mapping of the strain space by numerical simulations

Maximilian Zwicker[1], *Paulo A.F.* Martins[2], and *Chris Valentin* Nielsen[3*]

[1] Department of Civil and Mechanical Engineering, Technical University of Denmark, Denmark (now at Department of Mechanics Technology and Innovation, Group Advanced Manufacturing Engineering, Grundfos A/S, Bjerringbro, Denmark)
[2] IDMEC, Instituto Superior Técnico, Universidade de Lisboa, Portugal
[3] Department of Civil and Mechanical Engineering, Technical University of Denmark, Denmark

Abstract. Friction in metal forming is primarily determined by the real contact area between the workpiece surface asperities and the comparably flat tool surface. Asperities flatten due to normal loading, and subsurface strains heavily influence the degree of flattening. This work employs a three-dimensional numerical model based on the irreducible finite element flow formulation to determine the flattening of one pyramidal asperity unit cell. The flattening is simulated under normal loading combined with different biaxial in-plane subsurface strains. The numerical model was validated against existing experimental data available for plane strain and balanced biaxial strain states. The results of real contact area ratios were subsequently expanded to other ratios of the in-plane principal strains to map the entire strain space typical of forming limit diagrams.

Keywords: Friction modelling; Asperity flattening; In-plane strains; Numerical simulation.

1 Introduction

Friction in sheet metal forming largely depends on the real contact area between the sheet surface asperities and the comparably smooth tool surface. The evolution of the surface topography and, thus, the real contact area largely determines friction during forming processes. Therefore, a fundamental understanding of the mechanisms behind asperity flattening is required to estimate friction in sheet forming processes.

The importance of asperity flattening to friction in metal forming processes has been understood since the 1940s when Bowden and Tabor [1], Ernst and Merchant [2], and Holm [3] laid the foundation for the first quantitative theory of dry friction, the adhesion theory. Bowden and Tabor [1] already pointed out that friction cannot be considered only a surface phenomenon. Fogg [4] experimentally confirmed this by showing a reduction in measured hardness when combining hardness indentation with subsurface straining by in-plane stretching. The additional in-plane stresses result in a reduction of the necessary yield pressure and, therefore, asperity deformation results in further flattening to satisfy force equilibrium by larger real contact area and eventual strain hardening.

Research on asperity flattening due to combined normal loading and in-plane subsurface straining has been conducted by Sheu and Wilson [5], Sutcliffe [6], Wang et al. [7], Nielsen et al. [8], and Zwicker et al. [9] with the model asperity method. Shisode et al. [10] performed experiments on real surfaces, confirming the observations made on model asperities. Findings on model asperities can be transferred qualitatively to real surfaces, as argued by Zwicker et al. [11]. The above-mentioned research was carried out under plane strain or uniaxial stress conditions.

Since sheet metal forming combines a variety of strain states, it is crucial to investigate asperity flattening under normal loading combined with biaxial in-plane subsurface strains. The results may ultimately be implemented in friction models used in numerical simulations.

Zwicker et al. [12] presented a test apparatus that was inspired by the Marciniak-Kuczynski test principle. They combined the sheet formability test set-up with a center punch to enable the investigation of asperity flattening under combined normal loading and biaxial subsurface strains. In different experimental studies [12,13], it was observed that principal strain ratios of less than 0, i.e. plane strain, was not achievable for the applied level of normal load. This limitation of the strain space stems from the competing effects of thinning due to elongation, widening due to normal loading, and friction, causing resistance to any width change. Zwicker et al. [14] confirmed the strain space limitation analytically. However, the reality of sheet forming includes asperity flattening under in-plane principal strain ratios less than 0, i.e., elongation along the major strain and narrowing along the minor strain. It is, therefore, necessary to investigate the entire strain space to further advance the understanding of asperity flattening.

* Corresponding author: cvni@dtu.dk

In this work, the authors present a numerical model that overcomes the limitation of the strain space. With this model, it was possible to study the effect of negative in-plane subsurface principal strain ratios on the flattening of asperities. The numerical model considered pyramidal model asperities, and results were validated against experiments with pyramidal model asperities by Zwicker et al. [13].

2 Numerical model

The simulation of the flattening of pyramidal model asperities was conducted in 3D using the in-house finite element computer software i-form. The software is based on the irreducible finite element flow formulation. Detailed information about the theory and computer implementation is provided in [15].

The geometry of the numerical model was built according to the experimental work by Zwicker et al. [13], which was also used for validation. They investigated the flattening of pyramidal model asperities under combined normal loading and biaxial in-plane subsurface strains in an experimental setup first presented by Zwicker et al. [12]. The setup combines the Marciniak-Kuczynski test principle with a center punch, as schematically presented in Fig. 1, to enable the investigation of asperity flattening under biaxial in-plane strains combined with normal loading.

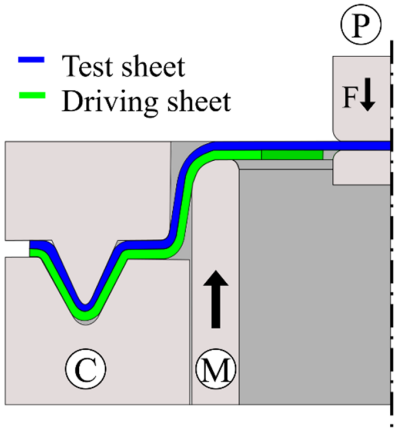

Fig. 1. Test principle with a center punch (P) combined with the Marciniak-Kuczynski test principle, where tool (C) is the clamping unit and tool (M) is the punch realizing the in-plane subsurface strains (arrows indicate directions of movement or direction of acting normal force)**.**

The experiments investigated the flattening of 381 pyramidal asperities with a flank angle γ = 10° and a base of 1.5 mm by 1.5 mm as shown in Fig. 2, where the simulation unit cell is also defined. The asperities were machined into 2.5 mm thick AA1050-H14 sheets with the Hollomon flow stress curve shown in Eq. (1).

$$\sigma = C\varepsilon^n = 122.6\varepsilon^{0.022}(MPa) \quad (1)$$

The experiments were conducted under constant normal force F = 31.5 kN, resulting in a nominal pressure on the original test surface of q_0 = 36.8 MPa. The asperities were lubricated with zinc stearate. Experiments were carried out with a strain ratio β around 0 and 1, where β is defined in Eq. (2).

$$\beta = \frac{\varepsilon_{minor}}{\varepsilon_{major}} \quad (2)$$

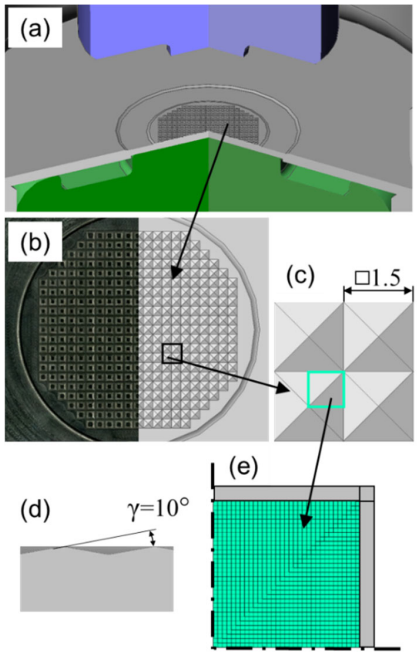

Fig. 2. Details of link between experiments and simulations shown by (a) 3D view of the center of the setup, (b) 2D view of the 381 asperities with flattened experiment (left) and undeformed model (right), (c) close-up of four asperities, (d) cross-section showing the flank angle, and (e) simulation unit cell seen from above. (a-d) are adapted from [13].

The numerical model considered a quarter pyramidal model asperity unit cell in 3D as defined in Fig. 2. The unit cell has the same dimensions as in the experiments, including the sheet thickness. Additional details are presented in Fig. 3. The numerical model of the asperity consists of 17303 elements (in the green part in Fig. 3) with the asperity being finely meshed and half the wavelength being discretized by 64 elements.

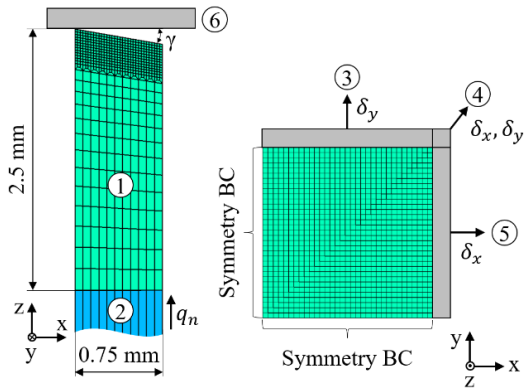

Fig. 3. Numerical model of a quarter pyramidal model asperity (1) with tools numbered (2-6) and tool directions of movement indicated by arrows.

The simulations were conducted with an isotropic material model applying the flow stress curve presented in Eq. (1). The normal pressure in the simulation was realized using a pressure boundary condition being applied to the bottom tool (2) with an initial linear pressure-build up over 100 time steps. After the normal pressure was stabilized, the tools (3), (4) and (5) were moved according to the applied strain ratio β. Tool (4) ensured that the nodes in the corner are displaced in both the x and y directions. Tool (6) remained stationary throughout the simulations. Between the flattening asperity tip and tool (6), friction according to the constant friction model with a friction factor m = 0.3 was considered. This friction factor is a typical value for soap lubricated aluminum [16]. The simulations were performed with a time step Δt = 0.001 s and a tool velocity in x and y of v = 0.01 mm/s for β = 1. The velocities in x were decreased for the tools (4) and (5) when simulating other β values.

After the simulations were finished, the real contact area ratio α, as presented in Eq. (3), was calculated. The apparent contact is the area spun between the symmetry boundaries and tools (3) and (5). The real contact area was calculated with a Python script. To calculate the area, the Python library alphashape [17] was used. It offers functions based on the mathematical idea of α-shapes to find the boundary of polygons consisting of a set of points. The set of points was found as the nodes, which were in contact with tool (6), as exemplarily shown in Fig. 4.

$$\alpha = \frac{real\ contact\ area}{aparent\ contact\ area} \tag{3}$$

Besides the real contact area ratio, the in-plane principal subsurface strains ε_y and ε_x were found from the displacement of tools (3) and (5), respectively. The subsurface equivalent strain ε_{eq} was calculated according to Eq. (4) based on the in-plane subsurface strains ε_x and ε_y and volume constancy. From here on, the in-plane principal subsurface strains will be referred to as simply "subsurface strains".

$$\varepsilon_{eq} = \sqrt{\frac{2}{3}\left({\varepsilon_x}^2 + {\varepsilon_y}^2 + \left(-\varepsilon_x - \varepsilon_y\right)^2\right)} \tag{4}$$

3 Results and discussion

Fig. 5 presents the subsurface major strain as a function of the subsurface minor strain, in the principal strain space, for all numerical simulations and the related experiments by Zwicker et al. [13]. Experimental results are presented for strain ratios β of around 0 and 1, and the numerical results are presented for different strain ratios β in the range of -0.5 to 1, i.e. a full principal strain space mapping from uniaxial tension (if there was no normal pressure) to balanced biaxial stretching.

Fig. 6 presents the real contact area ratio α as a function of the major subsurface strain and compares the experiments with β around 0 and 1 with the numerical simulation with β equal to 0 and 1. The real contact area ratio increases, with the major strain for both the experiments and simulations. The simulations and experiments are close to each other for low strains, but the simulated contact area ratio α is larger than the experimental one for larger strains. This can be explained by the difference in normal pressure at larger strains. While the experiments were conducted with a constant normal force F, i.e. a decreasing normal pressure with increasing apparent contact area, the numerical simulations were conducted with a constant normal pressure q, i.e., an increasing normal force F

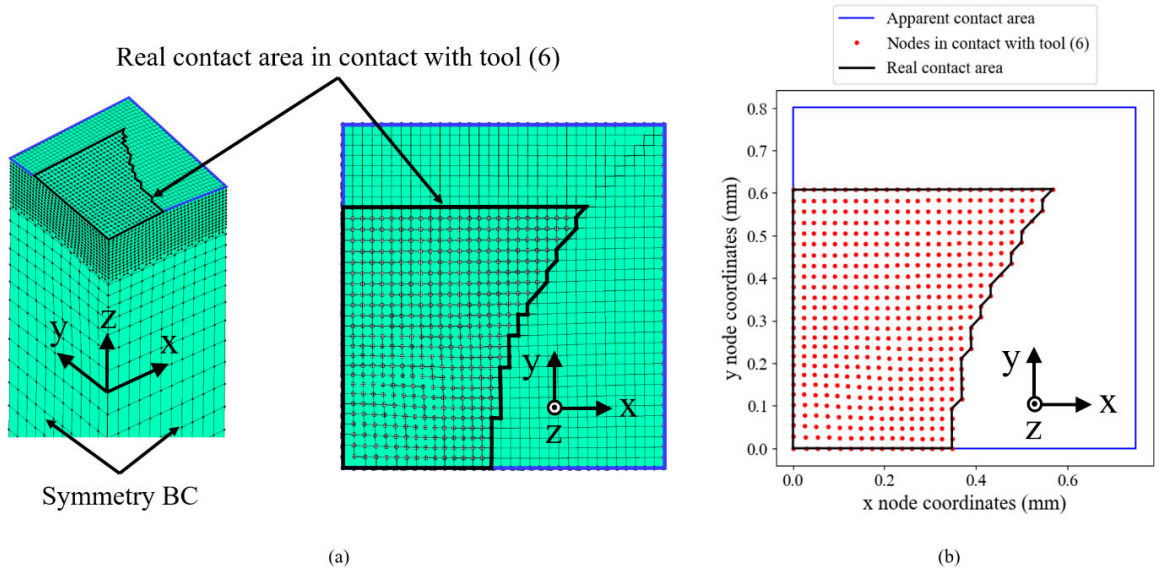

(a) (b)

Fig. 4. Example of the calculation of the real contact area ratio α for the numerical simulations: (a) 3D view of the numerical results for the strain ratio β=0 (ε_x=0, ε_y=0.067, α=0.43) with the real contact area marked with a black line and the apparent area with a blue line; (b) the real contact area of the simulation detected by the python code and the library alphashape.

with increasing apparent contact area. Both cases started with the same nominal normal pressure q_0.

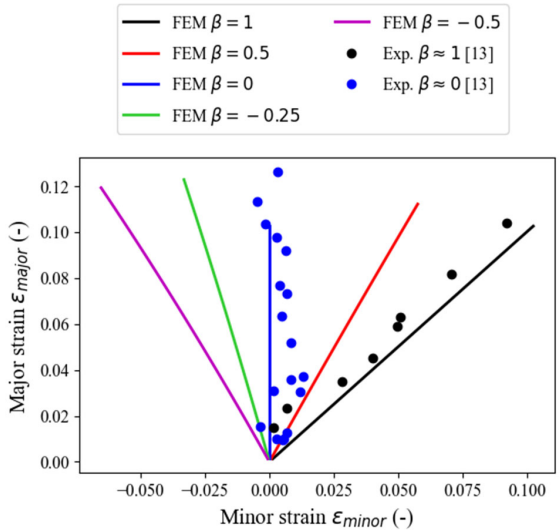

Fig. 5. Principal strain space showing the numerical simulation (FEM) results for strain ratios β mapping the strain space between -0.5 and 1, and the experimental (Exp.) results by Zwicker et al. [13] for β values of around 0 and 1.

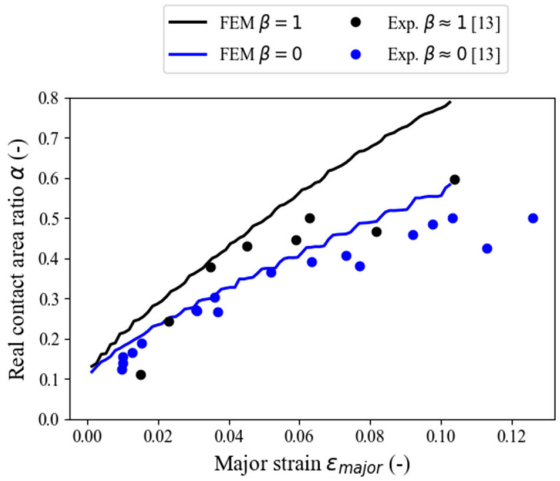

Fig. 6. Comparison of numerical and experimental results regarding the real contact area ratio α as a function of the major in-plane subsurface strain.

Fig. 7 presents the real contact area ratio α as a function of the major subsurface strain for the simulations with a strain ratio β ranging from -0.5 to 1. The real contact area ratio increases with the major subsurface strain for all five cases. The slope increases from β = -0.5 to β = 1 due to the in-plane tensile stresses reducing the necessary yield pressure for further asperity flattening.

Fig. 8 presents the real contact area ratio α as a function of the equivalent strain for all numerical simulations and the experiments from [13]. The real contact area ratio increases for both experiments and numerical simulations with the equivalent strain. The dependency of the strain ratio appears to be less than when shown against the major strain. The spread between the curves increases as the strain ratio decreases to negative values. Fig. 8 shows the same deviation of numerical and experimental real contact area ratios for higher strains, which, as explained above, results from the difference in normal pressure application.

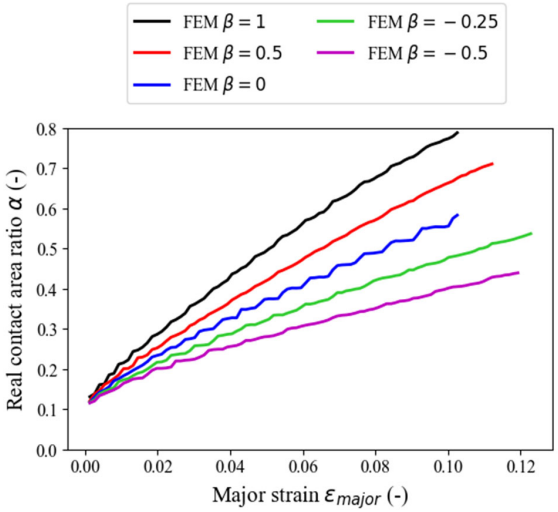

Fig. 7. The real contact area ratio α as a function of the major in-plane subsurface strain for the simulations with an in-plane strain ratio β ranging from -0.5 to 1.

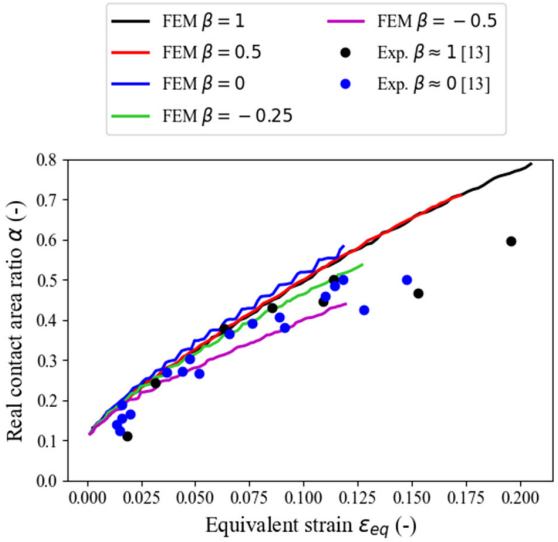

Fig. 8. The real contact area ratio α as a function of the equivalent strain for all numerical simulations (FEM) and experimental results by Zwicker et al. [13].

4 Conclusions

This work introduced a numerical model that enabled mapping of the full in-plane principal strain space during the flattening of pyramidal asperities. The following conclusions can be drawn:

- The pyramidal asperity unit cell was validated by experimental results.
- Simulations of an asperity unit cell can overcome the limitations of the strain space, which have

previously been observed in experiments. Thus, they enable studying effects on asperity flattening in the full strain ratio range, here from β = -0.5 to β = 1.

- Asperities were observed to flatten under combined normal loading and in-plane subsurface straining the most at a strain ratio β = 1 and the least for β = -0.5.

Future work may include the effects of higher strain hardening exponents and the influence of the flank angle on the sensitivity to the in-plane principal strain ratio. Further work on real surfaces with these loading conditions may contribute to advancing friction models used in numerical simulations.

Acknowledgments

Paulo Martins would like to acknowledge the support provided by Fundação para a Ciência e a Tecnologia (FCT) and IDMEC for its financial support via the project LAETA Base Funding (DOI: 10.54499/UIDB/50022/2020).

References

1. F.P. Bowden, D. Tabor. Nature **50**, 197 (1942)
2. H. Ernst, M.E. Merchant. In: Special Summer Conference on Friction and Surface Finish, 76 (1940)
3. R. Holm. Siemens-Werke Veröff. **17**, 400 (1938)
4. B. Fogg. Proc. Inst. Mech. Eng. Conf. Proc. **182**, 152 (1967)
5. S. Sheu, W.R.D. Wilson. Proc. 11th North American Manufact. Research Conf., 172 (1983)
6. M.P.F. Sutcliffe. Int. J. Mech. Sci. **30**, 847 (1988)
7. Z.G. Wang, Y. Yoshikawa, T. Suzuki, K. Osakada. Ann. CIRP **63**, 277 (2014)
8. C.V. Nielsen, P.A.F Martins, N. Bay. CIRP Ann. Manuf. Technol. **65**, 261 (2016)
9. M.F.R Zwicker, J. Spangenberg, N. Bay, P.A.F. Martins, C.V. Nielsen. Tribol. Int. **167**, 107416 (2021)
10. M. Shisode, J. Hazrati, T. Mishra, M. de Rooij, T. van den Boogaard. Friction **9**, 840 (2020)
11. M. Zwicker, N. Bay, C.V. Nielsen. Discov. Mech. Eng. **2**, 3 (2023)
12. M. Zwicker, N. Bay, C.V. Nielsen. Tribol. Int. **108**, 108249 (2023)
13. M. Zwicker, Ú. Arinbjarnar, M. Knoll, N. Bay, C.V. Nielsen. 14th Int. Conf. Technol. Plasticity, 12 (2023)
14. M. Zwicker, N. Bay, C.V. Nielsen. 9th JSTP Int. Sem. Precision Forging. 55 (2024)
15. C.V. Nielsen, P.A.F. Martins. Academic Press, Elsevier. 181 (2021)
16. N. Bay, T. Wanheim. Wear. **38**, 201 (1976)
17. K.E. Bellock. Python librabry alphashape 1.3.1. https://github.com/bellockk/alphashape. Downloaded 15.09.2023